NANO LETTERS

pubs.acs.org/NanoLett

Letter

Electronic Temperature and Two-Electron Processes in Overbias Plasmonic Emission from Tunnel Junctions

Alberto Martín-Jiménez, Koen Lauwaet, Óscar Jover, Daniel Granados, Andrés Arnau, Vyacheslav M. Silkin, Rodolfo Miranda, and Roberto Otero*

Cite This: *Nano Lett.* 2021, 21, 7086−7092

Read Online

ACCESS | Metrics & More | Article Recommendations | Supporting Information

ABSTRACT: The accurate determination of electronic temperatures in metallic nanostructures is essential for many technological applications, like plasmon-enhanced catalysis or lithographic nanofabrication procedures. In this Letter, we demonstrate that the electronic temperature can be accurately measured by the shape of the tunnel electroluminescence emission edge in tunnel plasmonic nanocavities, which follows a universal thermal distribution with the bias voltage as the chemical potential of the photon population. A significant deviation between electronic and lattice temperatures is found below 30 K for tunnel currents larger than 15 nA. This deviation is rationalized as the result of a two-electron process in which the second electron excites plasmon modes with an energy distribution that reflects the higher temperature following the first tunneling event. These results dispel a long-standing controversy on the nature of overbias emission in tunnel junctions and adds a new method for the determination of electronic temperatures and quasiparticle dynamics.

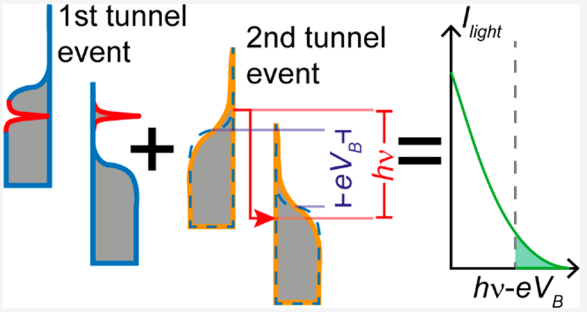

KEYWORDS: *Scanning tunneling electroluminescence, Electronic temperature, Plasmonic nanocavities, Quasiparticle lifetime, Ag(111) surface*

Solid state systems out of equilibrium can transiently sustain different temperatures for electronic and vibrational degrees of freedom.[1−7] Electron−electron interactions lead to a fast (∼1 ps) thermalization of the electronic energy distribution following excitation, while comparatively weak electron−phonon scattering only allows for full thermalization with the vibrational degrees of freedom after much longer times (≥100 ps).[1,3,6] Therefore, for intermediate time periods following an external excitation, the electronic cloud could have a temperature of thousands of Kelvin, while the atomic lattice remains at a much lower temperature.[1−7] This effect has been related to the enhanced catalytic and chemical activity of metallic nanoparticles under optical excitation,[8,9] and it is currently being exploited to optically increase the temperature of plasmonic nanoparticles or to improve the efficiency of metal−insulator−metal junctions as THz detectors.[10]

In this respect, a metallic tunnel junction traversed by an electric current is an example of a controllable, out-of-equilibrium solid nanostructure. Inelastic events during the electronic flow (both during the tunneling process and elsewhere) continuously pump energy into the electronic and vibrational degrees of freedom of the junction.[11−15] Such inelastic processes can increase the system's temperature[16] (electronic, vibrational, or both), but they can also create quasiparticle excitations such as localized surface plasmons which, upon radiative relaxation, lead to photon emission.[14,17−20] In principle, the maximum attainable photon energy for such electroluminescence processes is the applied bias voltage (the so-called quantum cutoff, see Figure 1b), but a clear radiation tail can be observed at higher photon energies, known as the overbias emission.[21−30] One explanation for the existence of such emission is blackbody radiation from the hot electron gas, the temperature of which would be higher than the lattice temperature due to the inelastic processes that electrons in the current flow experience.[22,26,28] Fitting this model to the experimental data requires temperatures of several thousand Kelvin to explain the observed overbias emission, a fact that has raised much interest lately.[22,26,28] However, an alternative model was also put forward to explain overbias emission: the existence of two-electron processes in which part of the energy of a first tunnel event is transferred to a second tunnel event, which can excite more energetic plasmons and, thus, lead to the emission of overbias photons.[23−25,27] This model is supported by the observed quadratic dependence of the overbias intensity with the

Received: March 9, 2021
Revised: June 15, 2021
Published: June 21, 2021

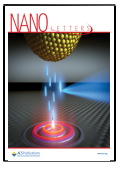

Downloaded via UNIV DEL PAIS VASCO on October 20, 2021 at 18:41:31 (UTC).
See https://pubs.acs.org/sharingguidelines for options on how to legitimately share published articles.

ACS Publications

© 2021 The Authors. Published by American Chemical Society

https://doi.org/10.1021/acs.nanolett.1c00951
Nano Lett. 2021, 21, 7086−7092

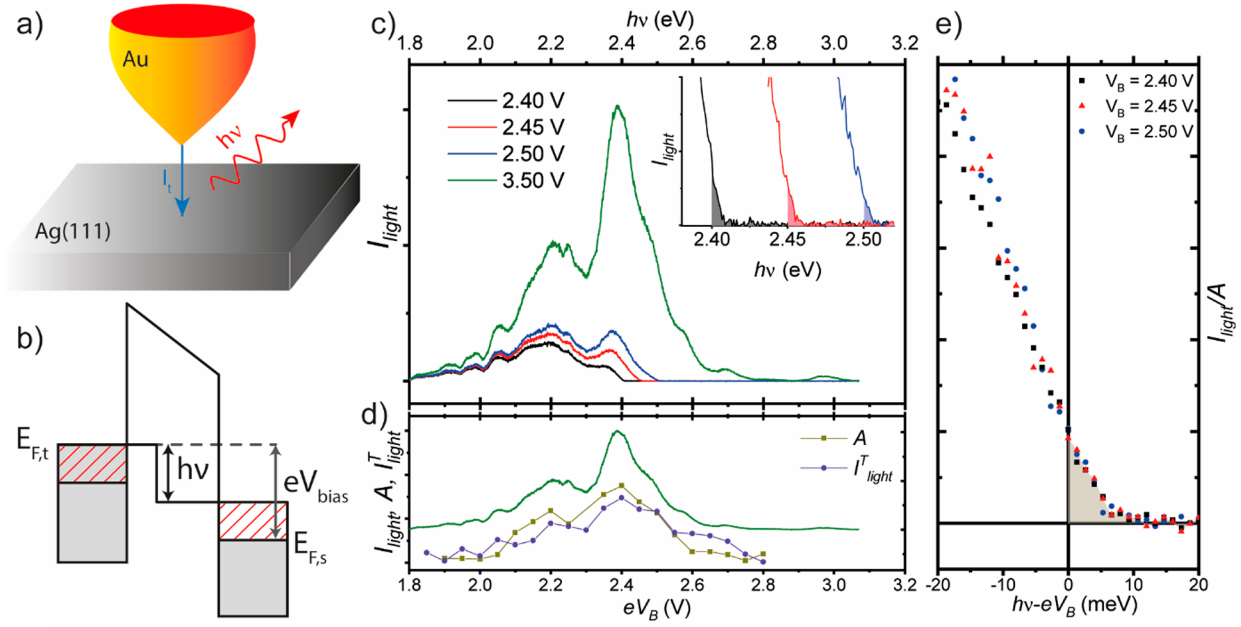

Figure 1. (a) Schematic representation of our experiment: a tunnel current flows from a Au STM tip to a Ag(111) surface exciting plasmons, the radiative decay of which leads to photon emission. (b) Level diagram showing that the width of the energy window of possible initial and final states of an inelastic tunnel process exciting a plasmon of energy $h\nu$ is $eV_B - h\nu$; i.e., for low photon energies, more inelastic transitions contribute to the emission. For photon energies higher than the bias voltage, inelastic processes linking occupied states in the tip and empty states in the sample become impossible. (c) Tunnel electroluminescence spectra recorded at 4.9 K with a bias voltage of 3.5 V, where all the relevant plasmonic cavity modes can be accessed by inelastic processes, and at lower voltages (2.4−2.5 V), demonstrating the suppression of intensity at photon energies larger that the applied bias. Inset: Zoom into the emission edge. The overbias emission tail is shadowed. (d) Comparison between the voltage dependence of the overbias amplitude (A, i.e., the light intensity at the cutoff) and total integrated emission (I^T_{light}, i.e., integrated light intensity at energies larger than the cutoff) with the fully developed spectra at 3.5 V. (e) Normalization of the emission edge spectra at different voltages by their respective amplitudes, A, makes the spectra voltage independent.

tunneling current,[23] and it casts shadows on the purely thermal interpretation of the overbias emission and on the temperature determination of the tunnel junction derived from it. Notice that a proper functional form for the cutoff function of the tunnel luminescence spectra in plasmonic junctions has only recently been described in the literature,[31] and thus, unambiguously distinguishing thermal and nonthermal effects has been difficult.

In this Letter, we describe a thorough experimental characterization of the overbias emission of a tunnel junction between a gold tip and a Ag(111) surface (see Figure 1a) as a function of the applied bias voltage, the tunneling current, and the junction temperature. Taking into consideration the expected shape of the electronic factor[31] close to the quantum cutoff, the analysis of these data demonstrates that the overbias emission spectra follows a thermal photon energy distribution, but only in terms of the excess energy above the tunnel bias; i.e., the bias voltage acts as the chemical potential for overbias photons. Electronic temperatures obtained from fitting to the mentioned distribution are found to match junction temperatures above 30 K and for currents below 10 nA but deviate significantly from them for lower temperatures and higher currents. Finally, we also find that the observed electronic temperatures scale with the average time between consecutive tunneling events, i.e., with the reciprocal of the tunnel intensity, following the same trend as the surface state electron lifetimes scale with the electron energies above the Fermi level. All these observations suggest a two-electron mechanism for the overbias emission process in which the first tunneling electron modifies the electronic temperature of the junction, while the photon emission from the second electron samples the electronic temperature at the time it tunnels. This mechanism, thus, finds common ground between the two controversial models for overbias emission and offers a unique tool to follow the thermalization and quasiparticle excitations dynamics with atomic spatial resolution and ps time resolution.

The concept of overbias emission is illustrated in Figure 1. Figure 1c displays the light intensity emitted from the tunnel junction held at 4.9 K for bias voltages of 2.4, 2.45, 2.5, and 3.5 V. Since these experiments are carried out with the feedback loop closed, tip−surface distances are different for each voltage and, thus, the plasmonic modes might also change. However, according to previous investigations, the voltage range explored in this paper is narrow enough to change tip−surface distances by no more than 1 Å, and the modification of the plasmonic properties (peak intensities and positions) is negligible.[31] Notice that the energy value 3.5 eV is larger than the photon energy of all the plasmonic modes. The corresponding spectrum shows peaks at all the relevant energies, with the light intensity being negligible at photon energies well below the applied bias. This fully developed spectrum contains information about the optical properties of the junction, including possible absorption effects at tip and junction. Notice that the width of the spectral features are in then range from 100 to 200 meVs. The energy values corresponding to the other three voltages sit in the middle of the plasmon-mode energies. Because the plasmonic modes of the cavity are excited by inelastic tunneling events, and the maximum energy that an electron can lose in such event is the applied bias voltage (see Figure 1b), the signal corresponding to the modes with energies higher than the bias voltage is strongly suppressed for the 2.4, 2.45, and 2.5 V cases. A careful

https://doi.org/10.1021/acs.nanolett.1c00951
Nano Lett. 2021, 21, 7086−7092

inspection of the data, however, reveals that this suppression is not complete (see inset in Figure 1c): A small but well-defined intensity tail can be observed at photon energies above the applied bias, extending about 10 meV to the region of higher photon energies, the so-called overbias emission. For the sake of comparison, the Fermi level broadening of the tunnel spectra at 4.9 K is about 1.5 meV ($\sim 4k_BT$), i.e., 1 order of magnitude smaller than the observed extension of the overbias region. Similar overbias can be observed at negative bias voltages, when electron flow from the sample to the tip (see SI3 in the Supporting Information).

In the following, we will experimentally characterize overbias emission through two parameters, the overbias amplitude, A, i.e., the light intensity at the so-called quantum cutoff condition, $h\nu = eV_B$, and the integrated intensity above the bias voltage, I^T_{light}. This last parameter is important because its dependence with the tunnel intensity has been previously described to be quadratic, supporting the two-electron interpretation of the origin of the overbias emission. Figure 1d shows A and I^T_{light} of a tunnel junction as a function of the bias voltage, demonstrating a very structured dependence with the voltage that closely follows the shape of the fully developed light spectrum recorded with a bias voltage of 3.5 V. Indeed, we find that, by normalizing the spectral distribution of the emission edges by A and plotting it versus the "excess" photon energy, $h\nu - eV_B$, all the data points fall into the same curve (Figure 1e), which follows a linear dependence for relatively large negative excess energies, tends to zero for relatively large positive excess energies, and shows a transition region of about 10 meV above and below zero excess energy (the quantum cutoff region, $h\nu \sim eV_B$).

We can rationalize this behavior by introducing the electronic factor that contributes to the observed tunnel electroluminescence spectra. Such spectra arise from the product of two factors, the local radiative photonic density of states of the plasmonic nanocavity at the tunnel junction, and the rate of inelastic transitions of tunneling electrons, which can be expressed as[31]

$$R_{inel}(h\nu, V_B) \sim \int_{-\infty}^{+\infty} \rho_T(E - eV_B + h\nu)\, f(E - eV_B + h\nu)\, \rho_S(E)(1 - f(E))\, \mathcal{T}_{inel}(E, h\nu, V_B)\, dE \quad (1)$$

where ρ_T and ρ_S are the tip and sample electronic density of states, respectively, $\mathcal{T}_{inel}$ is the inelastic transition function, and f is the Fermi–Dirac function of the electronic cloud in tip and sample. For photon energies sufficiently close to the applied bias, the density of states and transmission factors can be considered constant (assuming normal metal behavior, see section SI1 in the Supporting Information for more details). The remaining integral involving only the Fermi–Dirac functions can readily be performed (see section SI2 in the Supporting Information), and it yields

$$R_{inel}(h\nu \sim eV_B) \propto \frac{h\nu - eV_B}{e^{(h\nu - eV_B)/k_BT_{el}} - 1} \quad (2)$$

where T_{el} is the effective temperature of the electronic cloud determining the step width of the Fermi–Dirac function in eq 1. Notice that, in agreement with Figure 1e, R_{inel} in eq 2 is a function of the excess energy only. Moreover, its dependence with the excess energy follows qualitatively that described in Figure 1e for the experimental emission edges: at relatively large negative excess energies, it tends to the decreasing straight line $eV_B - h\nu$, while at large positive excess energies it tends to zero, with a transition region in the energy window of width $2k_BT_{el}$ around $h\nu = eV_B$. The overbias emission predicted by eq 2 results from the thermal broadening of the Fermi–Dirac distribution functions of tip and sample and, therefore, gauges the presence of electrons above the Fermi level and holes beneath the Fermi level in our system during the inelastic tunnel process. Notice that expression 2 corresponds to the average energy of an oscillatory mode of energy $h\nu - eV_B$ in thermal equilibrium with the electron cloud at temperature T_{el}; i.e., the bias voltage acts as the chemical potential for the creation of overbias photons, a result that should be taken into consideration when extracting temperatures from the shape of emission edges.

Figure 2a shows a comparison between the experimentally observed emission edges at a tunnel current intensity of 10 nA and the best fit according to eq 2 for different sample temperatures. This series was recorded with the same tip and tunneling parameters by measuring the tunnel electroluminescence spectra at equally spaced time intervals while slowly increasing the sample temperature in the STM. Sample temperatures (T_S) were measured with a diode placed on the back of the sample-holder receptacle. Here, the data have been normalized so that the slope of the edge at photon energies below the cutoff are the same for all spectra (see section SI2 in the Supporting Information for further discussion). The quantitative agreement between experimental data and eq 2 in Figure 2a is remarkable, supporting the interpretation of the overbias emission as arising from thermal broadening of the Fermi–Dirac distribution functions of tip and sample. Such agreement is further supported by Figure 2b, which shows the electronic temperatures obtained from the previous fit for different sample temperatures (the dashed line corresponds to $T_{el} = T_S$). This analysis demonstrates that for tunneling currents up to 10 nA and sample temperatures above 30 K, it is a good approximation to assume that electronic and sample temperatures coincide.

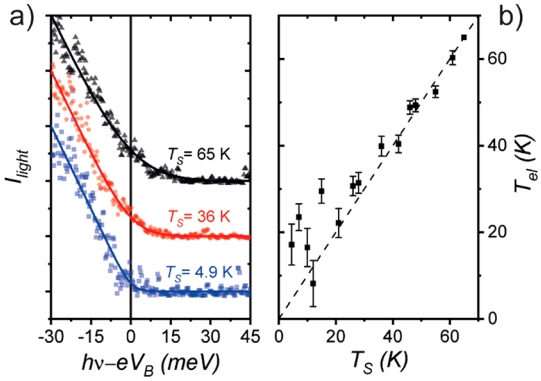

Figure 2. (a) Experimental emission edges measured at different sample temperatures (black squares 65 K, red dots 36 K, blue triangles 4.9 K) with a current of 10 nA and a bias voltage of 1.96 V, compared to the best fits to eq 2 (solid lines, same color code). (b) Electronic temperatures obtained from the previous fitting of the experimental data sets to eq 2 versus junction temperatures. Error bars are estimated from the standard deviation between the experimental data and the best fitted curve. The dashed line corresponds to $T_S = T_{el}$. There is a good correspondence between both measures for temperatures above 30 K, but not below.

https://doi.org/10.1021/acs.nanolett.1c00951
Nano Lett. 2021, 21, 7086−7092

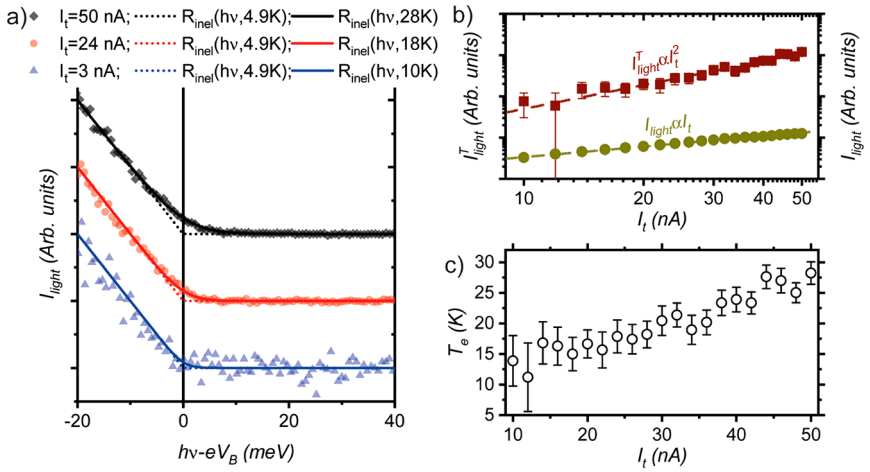

Figure 3. (a) Emission edges as a function of the tunneling current for a sample temperature of 4.9 K. Electroluminescence spectra were recorded with a bias voltage of 2 V. For comparison, the rate according to eq 2 is also plotted using the actual temperature of the junction (4.9 K, dashed lines) or the fitted temperature (solid lines). The overbias emission becomes more intense with increasing current. (b) Log−log plot of I^T_{light} (red) and the light intensity below the quantum cutoff (precisely at 1.98 eV, green) versus the tunneling current, revealing a linear dependence on the latter case but a quadratic dependence of the former. In this graph, we use the light intensity at a given photon energy instead of the integrated intensity below the quantum cutoff because for both cases there exists a proportionality relation with the tunnel current. (c) Dependence of the temperature obtained by fitting the experimental emission edges to eq 2 for the rates as a function of the tunneling current. The data shown in (b) and (c) include only data points for I_t > 10 nA because lower tunnel currents lead to spectra with relatively low signal-to-noise ratios, and both the integrated overbias intensities and integrated electronic temperatures show a rather large error bar.

Figure 2b, however, also shows some deviations between electronic and sample temperatures below T_S = 30 K for a tunnel intensity of 10 nA. The lower values obtained for the electronic temperatures as compared to other recent works might be related to our tunnel current being 3 orders of magnitude smaller than in previous studies.[22,26,28] It is also noticeable that, for such low currents, the lattice temperature at the junction is unlikely to be significantly different from the sample temperature: for example, a superconductive gap can be observed in InO_2 films (T_c = 1−3 K) with large conductivities of $0.5G_0$, whereas we run our experiments at a much smaller conductivity of $10^{-4}G_0$.[32] We are thus left with the option of attributing the discrepancies found in Figure 2b to differences between electronic and lattice temperatures.

As previously discussed, electronic and lattice temperatures can be significantly different in out-of-equilibrium systems, such as the tunnel junction being traversed by an electrical current. In this scenario, the rate of energy pumped into the system due to inelastic processes should increase with tunnel current, and so should the electronic temperature. To test this hypothesis, we have investigated the effect of the tunneling current in the spectral shape of the emission edge for a junction held at 4.9 K (Figure 3a, the data have been normalized to the slope, as the data in Figure 2a; more information in section SI2 in the Supporting Information). Indeed, we observe that the overbias emission edges can still be fitted by eq 2 in the range of currents between 1 and 50 nA, but the electronic temperatures and the integrated overbias light intensities obtained from the fitting of eq 2 to the experimental data do increase with increasing tunneling current (Figures 3b and c, respectively). The behavior at negative voltages is very similar (see SI3 and Figure S1 in the Supporting Information). In particular, the integrated light intensity in the overbias region depends quadratically on the tunneling current, a fact that usually implies that two-electron processes are essential to describe the effect. All these results indicate that, for relatively low junction temperatures and high current intensities, the thermal broadening of the Fermi−Dirac distribution functions in the tip and sample is larger than would be expected due to the sample temperature. Since the increased number of electrons above the Fermi level and holes below the Fermi level related to this elevated temperature scale with the tunnel current, it must arise from the scattering of hot carriers previously injected through the tunnel junction with other electrons and phonons of the sample.

This thermal broadening was attributed in previous works[24] to the creation of hot electrons and holes at the junction that decay via two electron (Auger-like) processes for very high tunneling currents of the order of μA.[24] However, at the relatively low tunnel intensities used here (1−50 nA), the time-lapse between two consecutive tunneling events is large enough ($\tau = e/I_t$, 3−160 ps) for the energy associated with the first electron excitation to have already been distributed among the rest of the electronic degrees of freedom (typically within 1 ps) but the full thermalization with the atomic lattice caused by electron−phonon scattering is still under way (typical time 100 ps). As sketched in Figure 4a, the second inelastic tunnel process might thus contribute to the overbias emission precisely because it would acquire the electronic temperature of the system at the time point of the second inelastic tunnel event and, indeed, this is higher than the lattice temperature. Moreover, the higher the tunnel current, the shorter the average lapse between consecutive tunnel events and therefore the thermalization time, explaining qualitatively the increase in the electronic temperature for increasing currents described in Figure 3c.

As the tunneling current in a wide bias voltage range is dominated by transitions to the Ag(111) surface state band electrons,[33,34] the characteristic lifetime of these excited surface state electrons can be used to trace the relation between the observed electronic temperature and the corresponding tunneling current. This inelastic lifetime is due to the inelastic processes of electron-photon scattering[35,36] and electron−electron interaction at finite temperatures,[36] and the

https://doi.org/10.1021/acs.nanolett.1c00951
Nano Lett. 2021, 21, 7086−7092

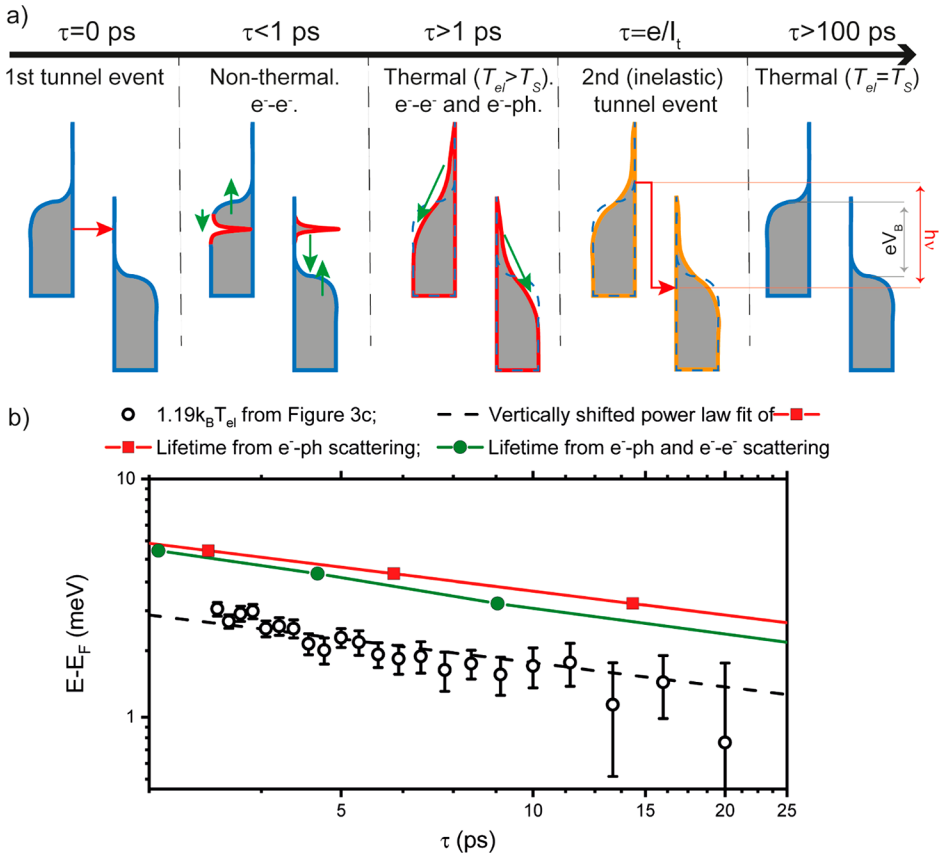

Figure 4. (a) Proposed mechanism for the observed overbias mechanism: the first tunnel event creates hot electrons and holes, leading to a nonequilibrium occupation of the electronic states. This nonequilibrium state decays rapidly due to the e^-−e^- scattering (green arrows) until the electron gas absorbs the excess energy of the hot carriers, thus increasing the electronic temperature with respect to that of the lattice. e^-−ph scattering events now provide the tool for the electron gas to equilibrate its temperature with that of the lattice (green arrows), but full thermalization is not achieved before 100 ps. A second tunnel event taking place in this time lapse could well contribute to an overbias emission higher than the expected one in terms of lattice temperature only, because of the higher electronic temperature. (b) Average energy of the electrons from the Fermi level estimated from the electronic temperatures in Figure 3c ($E - E_F = 1.19k_BT_{el}$) versus average time between tunneling events ($\tau = e/I_t$). The results are compared to calculations of the lifetime of electron quasiparticle in the Ag(111) surface state as a function of their energy, including the calculated e^-−e^- contribution and the e^-−ph scattering processes.[35,37]

corresponding self-consistent calculations are described in section SI5 in the Supporting Information. The average energy of hot electrons above the Fermi energy at a given electronic temperature can be calculated as $\langle E - E_F \rangle = \frac{\pi^2}{12\ln(2)} k_B T_{el} \approx 1.19 k_B T_{el}$ (see section SI4 in the Supporting Information). Thus, by converting from tunneling current into time span ($\tau = e/I_t$) and from electronic temperature to average energy separation from the Fermi level $\langle E - E_F \rangle$, we can reinterpret Figure 3c as a measure of the lifetimes of hot carriers as a function of electron energy. Figure 4b compares such reinterpretation of the data with self-consistent calculations of the lifetime of surface state electrons in Ag(111) including only electron−phonon scattering (red squares) or including also electron−electron scattering (green circles).

Inspection of Figure 4b reveals a power law dependence between average electron energy and time span between consecutive tunneling events, with an exponent close to −1/2 (slope in the log−log representation) which is compatible with that obtained from the self-consistent calculations of the quasiparticle excitations in the Ag(111) surface state (−0.42 for the calculation including e^-−ph and e^-−e^- scattering at finite temperatures). However, the values of the time span ($\tau = e/I_t$) extracted from the data are smaller than the calculated lifetime by about a factor of 2. We attribute this shorter time scale to the role of elastic scattering with defects, which is another contribution to electron lifetimes.

The previous argument relating the overbias analysis data and the electronic lifetime calculations strongly supports the view that overbias emission, in the range of tunneling parameters explored here, is caused by Fermi-level broadening of the emission cutoff energy due to a finite nonequilibrium electronic temperature. After the injection of a first tunneling electron, and at the instant of a second inelastic tunnel event, the value of the electronic temperature can be higher than the lattice temperature due to the incomplete thermalization of the electronic cloud. Notice that it can also be considered as a sort of a pump−probe mechanism, in which the first tunnel event creates an excitation of the system while the second tunnel event probes the fate of the excitation after some definite time fixed by the tunnel current intensity. From that point of view, we also provide STM with a time resolution between the ps and the ns. While innovative approaches are currently lowering the time resolution of STM below the picosecond by applying terahertz and petahertz pulses to the junction[38,39] and the application of electric pulses directly at the junction allows for the exploration of the nanosecond time scale,[40,41] the time

https://doi.org/10.1021/acs.nanolett.1c00951
Nano Lett. 2021, 21, 7086−7092

scale achievable through this technique has proven elusive to local measurement techniques.

To summarize, by means of a thorough experimental characterization and analysis of the overbias emission dependence on tunneling parameters, we have found the general shape of the emission edge spectrum and its dependence on temperature. This shape turns out to be compatible with thermal emission of plasmonic modes only when the bias voltage is considered as the chemical potential of the radiated photons. Our results show that, for junction temperatures above 30 K and tunnel currents of the order of tens of nanoamperes, thermal broadening effects are sufficient to explain the overbias emission. For lower junction temperatures and higher tunneling currents, however, a significant difference is found between the electronic temperatures determined from the overbias intensities and nominal junction temperatures. All these results support a two-electron mechanism in which the first tunneling electron creates an excitation in the system while the second one tests the thermalization of the system by the time it tunnels. This picture establishes connections between the two contradictory models previously published in the literature to explain overbias emission and opens the possibility to study the thermalization of nanoscale systems following injection of individual hot carriers with picosecond resolution, a method that can find applications for nanoscale metrology and for the optimization of photoactivated processes in nanostructures.

■ ASSOCIATED CONTENT

Supporting Information

The Supporting Information is available free of charge at https://pubs.acs.org/doi/10.1021/acs.nanolett.1c00951.

> Relation between the inelastic tunnel rate and the tunnel current for large and small voltages; functional form of the emission cutoff edge and normalization schemes; average energy of hot electrons at finite electronic temperatures; lifetime calculation method (PDF)

■ AUTHOR INFORMATION

Corresponding Author

Roberto Otero − *IMDEA Nanoscience, 28049 Madrid, Spain; Depto. de Física de la Materia Condensada and Condensed Matter Physics Center (IFIMAC), Universidad Autónoma de Madrid, 28049 Madrid, Spain;* orcid.org/0000-0001-6936-4003; Email: roberto.otero@uam.es

Authors

Alberto Martín-Jiménez − *IMDEA Nanoscience, 28049 Madrid, Spain;* Present Address: Max Planck Institute for Solid State Research, Heisenbergstr. 1, 70569 Stuttgart, Germany

Koen Lauwaet − *IMDEA Nanoscience, 28049 Madrid, Spain*

Óscar Jover − *IMDEA Nanoscience, 28049 Madrid, Spain; Depto. de Física de la Materia Condensada and Condensed Matter Physics Center (IFIMAC), Universidad Autónoma de Madrid, 28049 Madrid, Spain*

Daniel Granados − *IMDEA Nanoscience, 28049 Madrid, Spain;* orcid.org/0000-0001-7708-9080

Andrés Arnau − *Donostia International Physics Center (DIPC), 20018 San Sebastián/Donostia, Spain; Depto. de Polímeros y Materiales Avanzados: Física, Química y Tecnología, Facultad de Química, Universidad del País Vasco UPV/EHU, 20080 San Sebastián/Donostia, Spain; Centro de Fisica de Materiales CFM/MPC (CSIC-UPV/EHU), 20018 San Sebastián/Donostia, Spain*

Vyacheslav M. Silkin − *Donostia International Physics Center (DIPC), 20018 San Sebastián/Donostia, Spain; Depto. de Polímeros y Materiales Avanzados: Física, Química y Tecnología, Facultad de Química, Universidad del País Vasco UPV/EHU, 20080 San Sebastián/Donostia, Spain; IKERBASQUE, Basque Foundation for Science, 48009 Bilbao, Spain*

Rodolfo Miranda − *IMDEA Nanoscience, 28049 Madrid, Spain; Depto. de Física de la Materia Condensada and Condensed Matter Physics Center (IFIMAC), Universidad Autónoma de Madrid, 28049 Madrid, Spain*

Complete contact information is available at: https://pubs.acs.org/10.1021/acs.nanolett.1c00951

Author Contributions

The experiments were designed by K.L., A.M.-J., and R.O. The design and optimization of the experimental setup was carried out by A.M.-J.., K.L., and D.G. Experimental data collection was performed by A.M., K.L., and O.J. Lifetime calculations were developed by A.A. and V.M.S. R.M. and R.O. coordinated all the work, analyzed the data, and took a leading role in the writing of the manuscript. The manuscript was written through contributions of all authors. All authors have given approval to the final version of the manuscript.

Notes

The authors declare no competing financial interest.

■ ACKNOWLEDGMENTS

R.M. and R.O. acknowledge financial support from the Spanish Ministry for Economy and Competitiveness (Grants PGC2018-098613-B-C21, PGC2018-096047-B-I00), the regional government of Comunidad de Madrid (Grant S2018/NMT-4321), Universidad Autónoma de Madrid (UAM/48) and IMDEA Nanoscience. Both IMDEA Nanoscience and IFIMAC acknowledge support from the Severo Ochoa and Maria de Maeztu Programmes for Centres and Units of Excellence in R&D (MINECO, Grants SEV-2016-0686 and CEX2018-000805-M). R.O. acknowledges support from the excellence programme Echegaray, funded by the regional government of Madrid. A.A. and V.M.S. acknowledge support from the Spanish Ministry of Science and Innovation (Grants Nos. PID2019-103910GB-I00 and PID2019-105488GB-I00, respectively) and from the Projects of the Basque Government for consolidated groups of the Basque University, through the Department of Universities (Grant Nos. IT-1246-19 and IT-1164-19, respectively).

■ REFERENCES

(1) Shah, J. *Ultrafast Spectroscopy of Semiconductors and Semiconductor Nanostructures*; Springer-Verlag Berlin Heidelberg: Heidelberg, 1996.

(2) Faure, J.; Mauchain, J.; Papalazarou, E.; Marsi, M.; Boschetto, D.; Timrov, I.; Vast, N.; Ohtsubo, Y.; Arnaud, B.; Perfetti, L. Direct Observation of Electron Thermalization and Electron-Phonon Coupling in Photoexcited Bismuth. *Phys. Rev. B: Condens. Matter Mater. Phys.* **2013**, *88* (7), 1−9.

(3) Kemper, A. F.; Abdurazakov, O.; Freericks, J. K. General Principles for the Nonequilibrium Relaxation of Populations in Quantum Materials. *Phys. Rev. X* **2018**, *8* (4), 041009.

(4) Lisowski, M.; Loukakos, P. A.; Bovensiepen, U.; Stähler, J.; Gahl, C.; Wolf, M. Ultra-Fast Dynamics of Electron Thermalization, Cooling and Transport Effects in Ru(001). *Appl. Phys. A: Mater. Sci. Process.* **2004**, *78* (2), 165−176.
(5) Guo, C.; Rodriguez, G.; Taylor, A. J. Ultrafast Dynamics of Electron Thermalization in Gold. *Phys. Rev. Lett.* **2001**, *86* (8), 1638−1641.
(6) Maldonado, P.; Carva, K.; Flammer, M.; Oppeneer, P. M. Theory of Out-of-Equilibrium Ultrafast Relaxation Dynamics in Metals. *Phys. Rev. B: Condens. Matter Mater. Phys.* **2017**, *96* (17), 174439.
(7) Sun, C. K.; Vallée, F.; Acioli, L.; Ippen, E. P.; Fujimoto, J. G. Femtosecond Investigation of Electron Thermalization in Gold. *Phys. Rev. B: Condens. Matter Mater. Phys.* **1993**, *48* (16), 12365.
(8) Li, S.; Miao, P.; Zhang, Y.; Wu, J.; Zhang, B.; Du, Y.; Han, X.; Sun, J.; Xu, P. Recent Advances in Plasmonic Nanostructures for Enhanced Photocatalysis and Electrocatalysis. *Adv. Mater.* **2021**, *33*, 2000086.
(9) Dhiman, M. Plasmonic Nanocatalysis for Solar Energy Harvesting and Sustainable Chemistry. *J. Mater. Chem. A* **2020**, *8*, 10074−10095.
(10) Brongersma, M. L.; Halas, N. J.; Nordlander, P. Plasmon-Induced Hot Carrier Science and Technology. *Nat. Nanotechnol.* **2015**, *10* (1), 25−34.
(11) Stipe, B. C.; Rezaei, M. A.; Ho, W. Single-Molecule Vibrational Spectroscopy and Microscopy. *Science* **1998**, *280* (5370), 1732−1735.
(12) Heinrich, A. J.; Gupta, J. A.; Lutz, C. P.; Eigler, D. M. Single-Atom Spin-Flip Spectroscopy. *Science* **2004**, *306* (5695), 466−469.
(13) Lambe, J.; Jaklevic, R. C. Molecular Vibration Spectra by Inelastic Electron Tunneling. *Phys. Rev.* **1968**, *165* (3), 821−832.
(14) Lambe, J.; McCarthy, S. L. Light Emission from Inelastic Electron Tunneling. *Phys. Rev. Lett.* **1976**, *37* (14), 923−925.
(15) Persson, B. N. J.; Baratoff, A. Inelastic Electron Tunneling from a Metal Tip: The Contribution from Resonant Processes. *Phys. Rev. Lett.* **1987**, *59* (3), 339−342.
(16) Gapihan, E.; Hérault, J.; Sousa, R. C.; Dahmane, Y.; Dieny, B.; Vila, L.; Prejbeanu, I. L.; Ducruet, C.; Portemont, C.; MacKay, K.; Nozières, J. P. Heating Asymmetry Induced by Tunneling Current Flow in Magnetic Tunnel Junctions. *Appl. Phys. Lett.* **2012**, *100* (20), 202410.
(17) Berndt, R.; Gimzewski, J. K.; Johansson, P. Electromagnetic Interactions of Metallic Objects in Nanometer Proximity. *Phys. Rev. Lett.* **1993**, *71* (21), 3493−3496.
(18) Berndt, R.; Gimzewski, J. K.; Johansson, P. Inelastic Tunneling Excitation of Tip-Induced Plasmon Modes on Noble-Metal Surfaces. *Phys. Rev. Lett.* **1991**, *67* (27), 3796−3799.
(19) Rossel, F. F.; Pivetta, M.; Schneider, W.-D. Luminescence Experiments on Supported Molecules with the Scanning Tunneling Microscope. *Surf. Sci. Rep.* **2010**, *65* (5), 129−144.
(20) Kuhnke, K.; Große, C.; Merino, P.; Kern, K. Atomic-Scale Imaging and Spectroscopy of Electroluminescence at Molecular Interfaces. *Chem. Rev.* **2017**, *117* (7), 5174−5222.
(21) Pechou, R.; Coratger, R.; Ajustron, F.; Beauvillain, J. Cutoff Anomalies in Light Emitted from the Tunneling Junction of a Scanning Tunneling Microscope in Air. *Appl. Phys. Lett.* **1998**, *72* (6), 671−673.
(22) Downes, A.; Dumas, P.; Welland, M. E. Measurement of High Electron Temperatures in Single Atom Metal Point Contacts by Light Emission. *Appl. Phys. Lett.* **2002**, *81* (7), 1252−1254.
(23) Schull, G.; Néel, N.; Johansson, P.; Berndt, R. Electron-Plasmon and Electron-Electron Interactions at a Single Atom Contact. *Phys. Rev. Lett.* **2009**, *102* (5), 057401.
(24) Schneider, N. L.; Johansson, P.; Berndt, R. Hot Electron Cascades in the Scanning Tunneling Microscope. *Phys. Rev. B: Condens. Matter Mater. Phys.* **2013**, *87* (4), 045409.
(25) Xu, F.; Holmqvist, C.; Belzig, W. Overbias Light Emission Due to Higher-Order Quantum Noise in a Tunnel Junction. *Phys. Rev. Lett.* **2014**, *113* (6), 066801.
(26) Buret, M.; Uskov, A. v.; Dellinger, J.; Cazier, N.; Mennemanteuil, M. M.; Berthelot, J.; Smetanin, I. v.; Protsenko, I. E.; Colas-Des-Francs, G.; Bouhelier, A. Spontaneous Hot-Electron Light Emission from Electron-Fed Optical Antennas. *Nano Lett.* **2015**, *15* (9), 5811−5818.
(27) Peters, P. J.; Xu, F.; Kaasbjerg, K.; Rastelli, G.; Belzig, W.; Berndt, R. Quantum Coherent Multielectron Processes in an Atomic Scale Contact. *Phys. Rev. Lett.* **2017**, *119* (6), 066803.
(28) Cui, L.; Zhu, Y.; Abbasi, M.; Ahmadivand, A.; Gerislioglu, B.; Nordlander, P.; Natelson, D. Electrically Driven Hot-Carrier Generation and Above-Threshold Light Emission in Plasmonic Tunnel Junctions. *Nano Lett.* **2020**, *20* (8), 6067−6075.
(29) Ekici, E.; Kapitza, P.; Bobisch, C. A.; Möller, R. Electron-Induced Photon Emission above the Quantum Cutoff Due to Time-Energy Uncertainty. *Opt. Lett.* **2017**, *42* (22), 4585.
(30) Kalathingal, V.; Dawson, P.; Mitra, J. Scanning Tunnelling Microscope Light Emission: Finite Temperature Current Noise and over Cut-off Emission. *Sci. Rep.* **2017**, *7* (1), 3510−3530.
(31) Martín-Jiménez, A.; Fernández-Domínguez, A. I.; Lauwaet, K.; Granados, D.; Miranda, R.; García-Vidal, F. J.; Otero, R. Unveiling the Radiative Local Density of Optical States of a Plasmonic Nanocavity by STM. *Nat. Commun.* **2020**, *11* (1), 1021.
(32) Dubouchet, T.; Sacépé, B.; Seidemann, J.; Shahar, D.; Sanquer, M.; Chapelier, C. Collective Energy Gap of Preformed Cooper Pairs in Disordered Superconductors. *Nat. Phys.* **2019**, *15*, 233−236.
(33) Li, J.; Schneider, W. D.; Berndt, R.; Bryant, O. R.; Crampin, S. Surface-State Lifetime Measured by Scanning Tunneling Spectroscopy. *Phys. Rev. Lett.* **1998**, *81* (20), 4464−4467.
(34) Kliewer, J.; Berndt, R.; Chulkov, E. v.; Silkin, V. M.; Echenique, P. M.; Crampin, S. Dimensionality Effects in the Lifetime of Surface States. *Science* **2000**, *288* (5470), 1399−1402.
(35) Eiguren, A.; Hellsing, B.; Reinert, F.; Nicolay, G.; Chulkov, E. v.; Silkin, V. M.; Hüfner, S.; Echenique, P. M. Role of Bulk and Surface Phonons in the Decay of Metal Surface States. *Phys. Rev. Lett.* **2002**, *88* (6), 066805.
(36) Benedek, G.; Bernasconi, M.; Campi, D.; Silkin, I. v.; Chernov, I. P.; Silkin, V. M.; Chulkov, E. v.; Echenique, P. M.; Toennies, J. P.; Anemone, G.; al Taleb, A.; Miranda, R.; Farías, D. Evidence for a Spin Acoustic Surface Plasmon from Inelastic Atom Scattering. *Sci. Rep.* **2021**, *11*, 1506.
(37) Eiguren, A.; Hellsing, B.; Chulkov, E. v.; Echenique, P. M. Phonon-Mediated Decay of Metal Surface States. *Phys. Rev. B: Condens. Matter Mater. Phys.* **2003**, *67* (23), 235423.
(38) Cocker, T. L.; Jelic, V.; Gupta, M.; Molesky, S. J.; Burgess, J. A. J.; Reyes, G. D. L.; Titova, L. v.; Tsui, Y. Y.; Freeman, M. R.; Hegmann, F. A. An Ultrafast Terahertz Scanning Tunnelling Microscope. *Nat. Photonics* **2013**, *7*, 620−625.
(39) Garg, M.; Kern, K. Attosecond Coherent Manipulation of Electrons in Tunneling Microscopy. *Science* **2020**, *367* (6476), 411−415.
(40) Loth, S.; Etzkorn, M.; Lutz, C. P.; Eigler, D. M.; Heinrich, A. J. Measurement of Fast Electron Spin Relaxation Times with Atomic Resolution. *Science* **2010**, *329* (5999), 1628−1630.
(41) Kemiktarak, U.; Ndukum, T.; Schwab, K. C.; Ekinci, K. L. Radio-Frequency Scanning Tunnelling Microscopy. *Nature* **2007**, *450*, 85−88.

https://doi.org/10.1021/acs.nanolett.1c00951
Nano Lett. 2021, 21, 7086−7092